Biological Response to the Dynamic Spectral-Polarized Underwater Light Field

PI: Molly E. Cummings
Section of Integrative Biology C0930
University of Texas
Austin, TX 78712
phone: (512) 471-5162 fax: (512) 471-3878 email: mcummings@mail.utexas.edu

Co-PI: Samir Ahmed (City College of New York)
Co-PI: Heidi Dierssen (University of Connecticut)
Co-PI: Alexander Gilerson (City College of New York)
Co-PI: William F. Gilly (Stanford University)
Co-PI: George Kattawar (Texas A & M University)
Co-PI: Brad Seibel (University of Rhode Island)
Co-PI: James Sullivan (University of Rhode Island)

Award Number: N000140911054
http://www.bio.utexas.edu/research/cummingslab/

LONG-TERM GOALS

Camouflage in marine environments requires matching all of the background optical properties: spectral, intensity and polarization components─ all of which can change dynamically in space and time. Current research suggests that polarization detection is more sensitive than other conventional detection methods in scattering media such as the ocean, hence underscoring the need to develop polarized camouflage technology. Our research investigates the biological challenge of camouflage in the near-shore littoral zone and near-surface marine environments in two distinct water types found in coastal environments around the globe (oligotrophic and eutrophic) with particular emphasis on the polarization properties. We aim to characterize the dynamic light field along with the behavioral and cellular response of camouflaging animals in these environments. Our long-term goal is to identify the biological pathways for concealment against the underwater spectral-polarized light field enabling us to identify design principles for future naval camouflage.

OBJECTIVES

(1) Measure and model the spectral-polarized light field in near-shore and near-surface environments

(2) Characterize the biological camouflage response of organisms to these dynamic optical fields

(3) Identify the internal controls and structural mechanisms that coordinate the camouflage response

Report Documentation Page

Form Approved
OMB No. 0704-0188

1. REPORT DATE	2. REPORT TYPE	3. DATES COVERED
2012	**N/A**	**-**

4. TITLE AND SUBTITLE	5a. CONTRACT NUMBER
Biological Response to the Dynamic Spectral-Polarized Underwater Light Field	5b. GRANT NUMBER
	5c. PROGRAM ELEMENT NUMBER
6. AUTHOR(S)	5d. PROJECT NUMBER
	5e. TASK NUMBER
	5f. WORK UNIT NUMBER
7. PERFORMING ORGANIZATION NAME(S) AND ADDRESS(ES) **Section of Integrative Biology C0930 University of Texas Austin, TX 78712**	8. PERFORMING ORGANIZATION REPORT NUMBER
9. SPONSORING/MONITORING AGENCY NAME(S) AND ADDRESS(ES)	10. SPONSOR/MONITOR'S ACRONYM(S)
	11. SPONSOR/MONITOR'S REPORT NUMBER(S)

12. DISTRIBUTION/AVAILABILITY STATEMENT
Approved for public release, distribution unlimited

13. SUPPLEMENTARY NOTES
The original document contains color images.

14. ABSTRACT

15. SUBJECT TERMS

16. SECURITY CLASSIFICATION OF:			17. LIMITATION OF ABSTRACT	18. NUMBER OF PAGES	19a. NAME OF RESPONSIBLE PERSON
a. REPORT	b. ABSTRACT	c. THIS PAGE			
unclassified	**unclassified**	**unclassified**	**SAR**	**20**	

APPROACH

Our first aim is to **measure and model the underwater spectral-polarized light field in distinct water types**. We characterize the light field by the simultaneous deployment of a comprehensive optical suite including underwater video-polarimetry (full Stokes vector video-imaging camera custom-built Cummings; and "SALSA" (Bossa Nova Technologies, CA) Gilerson), inherent optical properties, (LISST by Dierssen), hyper-spectral multi-angular Stokes vector spectroradiometry (Gilerson,Ahmed), and the volume scattering function measures (MASCOT by Sullivan). These measurements will be used to refine development of, and make comparisons to, theoretical expectations from a fully 3-D radiative transfer model that solves for each of the polarization elements of the Mueller matrix transformation of the Stokes vector by (Kattawar). The first modeling objective of this proposal is to calculate the complete Mueller matrix/Stokes vector for any set of oceanic and atmospheric conditions for any region of the ocean. We will then use this modeling approach (*i*) to predict the 3-D light field; (*ii*) to calculate experimental conditions to measure biological responses; and (*iii*) to investigate the nature of the light field as it interacts with cells within the skin. Our approach is to develop a 3-D Monte Carlo model with full Mueller matrix treatment.

During field operations, we couple polarimetry measurements of live, free-swimming animals in their environments with a full suite of optical measurements (mentioned above) to completely characterize the **biological response to dynamic optical environments** (Cummings, Gilerson, Dierssen, Sullivan, Seibel, Ahmed)**.** We also restrain live, awake animals to take polarimetry measurements (in the field and laboratory) under a complete set of viewing angles and incident polarization light fields. We use Mueller matrix modeling to determine the specific Mueller matrix elements of animals that differ from those of conventional structures currently deployed for open ocean camoflauge (e.g. standard mirror). Furthermore, we examine *in vivo* "flickering" activity on the skin of several species of squid and its relationship to background matching (wave-induced fluctuations of the light field) (Gilly).

We **identify the internal control of these field-studied organisms and structural mechanisms that coordinate the camouflage response** by (a) characterizing different tissue layers and organelles associated with different species occupying a diverse array of marine habitats using a combination of light and SEM microscopy (Cummings, Gilly), (b) examining both iridophore and chromatophore control processes and the local vs peripheral control features using both pharmacological and electrical stimulation techniques (Gilly, Cummings), and (c) developing a novel 3D Monte Carlo model to describe how the spectral-polarized light field interacts with cells within the skin (Kattawar).

WORK COMPLETED

a) The Backward Monte Carlo code for the ocean was completed and checked by running several canonical cases which could be compared with other independent methods. (Kattawar)

b) Finished housing and integration of a new underwater spectrometer designed to measure benthic reflectance of the seafloor (Dierssen)

c) Participated in 3rd year MURI review including field planning meeting in November 2011 in Austin, TX (Cummings, Dierssen, Kattawar, Sullivan, Gilerson, Ahmed, collaborator Twardowski, Seibel, Gilly)

d) Upgraded the SALSA videopolarimeter camera to a video frame rate up to 15 frames/s (from previous 4 frames/s) to study fast changing processes in water (Gilerson)

e) Completed 5 field campaigns in different locations: Texas (Cummings, Seibel); Curacao (Cummings, Gilerson, Sullivan, Dierssen, Ahmed, Twardowski, Seibel); California (Dierssen), Gulf of California (Gilly), Long Island, NY (Gilerson, Ahmed)

f) Completed the model of polaro-crypsis with respect to the measured Mueller matrix of our biomimicry model, the lookdown, *Selene vomer* (Cummings)

g) Data from two 2011 field campaigns that measured polarization characteristics of light in shallow water environments with seagrass, coral reef and sand bottoms were analyzed together with simulations obtained using a vector radiative (RT) transfer code RayXP. Group paper is in final preparation (Gilerson, Ahmed, Sullivan, Twardowski, Dierssen, Cummings)

h) Developed and calibrated (Fig 1) a customized sensor package for video polarimeter cameras that measures compass heading, camera pitch, camera roll, ambient light, temperature, and depth (Cummings)

i) Conducted field campaign to Curacao (July 2012) to test our biological polaro-cryptic mirror hypothesis for open ocean camouflage including the following optical measurements: spectral stokes vector radiometry and polarization videoimagery, IOPs and VSF with MASCOT, partical size distributions with LISST, remote sensing reflectance with ASD and HTSRB, and benthic reflectance spectrometery (Gilerson, Sullivan, Cummings, Dierrsen, Twardowski)

j) Measured camouflaged polarimetry and hyperspectral response to live squid, teleost fish, and crab species in controlled laboratory conditions during two field campaigns (Port Aransas, TX; January 2012 and Curacao July 2012) to determine dynamic response to changes in the polarized light field (Cummings, Seibel,Dierssen)

k) Compared flickering in field data from the squid *Dosidicus* with downwelling irradiance in the Gulf of California (Gilly).

l) Conducted preliminary hyperspectral reflectance measurements and imaging of sea hare camouflage in eelgrass (California July 2012; Dierssen).

m) Extended previous work concerning the effects of tetrodotoxin on chromatophore function, along with cytochemical localization, to *Sthenoteuthis* and denervated *Doryteuthis*. (Gilly)

n) The backscattering properties of an iridosome are characterized using first-principle simulation (DDA), and compared with semi-infinite plates. (Kattawar)

o) The inner structure of a leucophore are analyzed and identified using the discrete Fourier transformation (DFT) method. The diffuse reflection of the leucophore system is simulated using a Monte Carlo method. The refractive index and the angular reflectance are obtained. (Kattawar)

p) Characterized the structure and organization of the iridophore layers in a number of species of marine fish by light and scanning electron microscopy (Cummings)

q) Completed cloning of five opsin genes (rhodopsin plus four cone opsins (LWS, Rh2, SWS1, SWS2)) from lookdown (*Selene vomer*) eye tissue and three opsins (rhodopsin, LWS, SWS1) from lookdown skin tissue (Cummings)

RESULTS

(1) Our Mueller matrix modeling of lookdown polarimetry reflectance shows that this fish has optimal polaro-crypsis performance (Fig 2) and outperforms conventional strategies for open ocean camouflage (e.g. vertical mirror) as well as fish occupying more turbid environments (e.g. seagrass). This open ocean fish achieves excellent polaro-crypsis by selectively depolarizing its reflectance, as well as modifying the angle of incident polarized light, in a context-specific fashion. The lookdown strategy represents a novel strategy for polaro-crypsis in the open ocean (Brady et al., submitted).

(2) Our comparison of the hyperspectral polarization characteristics of light in shallow waters with different substrates (seagrass, sand, coral reef) reveal that in most cases a a Lambertian unpolarized bottom with proper spectral reflectance represents an appropriate model to determine polarization characteristics of light in the water column (Fig. 3)

(3) Based on extensive simulations of polarization characteristics of light in a broad range of water environments (RayXP code) developed polarization technique for the retrieval of the attenuation/absorption ratio of water from the polarized measurements of water leaving radiance and analyzed its sensitivity to the slope of particle size distribution, illumination and viewing conditions (Fig.4; Ibrahim et al, *accepted, Optics Express*).

(4) The continued use of the POLMOD-MASCOT device during all MURI field cruises has greatly added to the first comprehensive data set ever recorded for VSF and polarized scattering in the oceans within undisturbed particle fields. Field data of the degree of linear polarization (DoLP) for natural particle fields are being compared to modeled DoLPs from theoretical particle fields using both spherical and non-spherical particles (asymmetric polyhedra) as model inputs (Figs. 5 and 6). Initial results indicate that polarized scattering is more variable than currently thought, Lorenz-Mie theory is a reasonable first order approximation for linearly polarized scattering, especially for surface waters, and scaling Rayleigh scattering for linear polarization is not adequate (Twardowski-Sullivan).

(5) Dynamic camouflage on the scale of 12-48hrs was observed in the Sargassum crab, P. sayi, using hyperspectral imaging (Fig 7; Dierssen)

(6) Behavioral testing of the Atlantic needlefish (*Strongylura marina*) and the yellowtail snapper (*Ocyurus chrysurus*) indicate that polarization reflectance, and polaro-crypsis, is under peripheral control and does not appear to be modulated by the CNS (Fig 8; Ruddick et al., in prep). Atlantic needlefish (a near-surface fish) outperform yellowtail snapper (found near coral reefs and mid-water) in terms of polaro-crypsis suggesting that habitat may play a role in tuning physiological features used in polarized camouflage (Cummings).

(7) We numerically studied the backscattering properties of an iridosome using the Discrete Dipole Approximation (DDA) method, and compared the results with their semi-infinite plate counterparts. From these comparisons, we provided the criteria for using the semi-infinite approximations to estimate iridosome properties. The results for the backscattering efficiency are shown in Fig. 9. (Kattawar)

(8) Using discrete Fourier analysis (DFT) on the leucosome position data, we found that there is no spatial correlation between leucosomes inside leucophore cell (Fig. 10). This suggests a leucophore is a random system. (Kattawar)

(9) We simulated the diffuse reflection of a lucophore system. From the comparison of measured reflection and numerical simulation results, we identified the leucosome refractive index should be around 1.50 to 1.54. (Fig 11). We also obtained the angular reflectance, and it is shown to be close to a Lambertian surface (Fig 12). (Kattawar)

(10) Temporal characteristics of flickering in Dosidicus are comparable to those of fluctuations in intensity of downwelled blue light (Fig 13A, data from M.Darecki and D. Stramski, Scripps), suggesting a possible functional role of dynamic crypsis for flickering. Similar behavior was observed in lab observations of free-swimming *Sthenoteuthis* (not illustrated) and *Doryteuthis* (Fig. 13B). (Gilly)

(11) Responses from electrically stimulated chromatophores in Sthenoteuthis and the effects of tetrodoxin (Fig 14) were similar to those previously reported for *Dosidicus*. Preliminary results with *Doryteuthis* suggest that peripheral control of chromatophores is only evident after denervation. (Gilly)

(12) A complex network of neural processes within the chromatophore layer of the skin (*Doryteuthis*) was found that could indicate a peripheral nerve-net distinct from the descending motor supply (Fig 15A). A high degree of branching in radial muscle fibers was evident (Gilly).

(13) Light and SEM microscopy showed great variation in iridophore layering structure across marine fish species. In most species, iridophores are present in the epidermis that are closely associated with the scales and in the dermis, but are absent in the lookdown and Atlantic needlefish. Two distinct iridophore types are observed in the dermis of the lookdown and form two distinct layers, both in the dermis and adjacent to each other (Fig 16, 17). These different iridiphore types and layers may be responsible for the unique polarization reflectances of this species. Further research will determine whether iridophore layer topography is predictable by fish ecotype. (Cummings)

(14) Our opsin research with the lookdowns indicate that the lookdown has the full complement of retinal opsins typically found in teleost eye tissue coupled with the most complex array of peripheral opsin expression yet identified in a teleost species. Lookdown fish express three distinct opsin types in skin tissue, giving it the potential to detect low light (rhodopsin), red wavelength (LWS) and UV light (SWS1) at a peripheral level (Cummings).

IMPACT/APPLICATIONS

1. The reflectance of semi-infinite plates can be calculated analytically and efficiently. Using our criterion we can provide guidance on which range the results for semi-infinite plates can be used to estimate the reflectance of an iridosome, and therefore increase the accuracy and efficiency in modeling iridosomes.

2. The studies on leucophores broadened our understanding of their structure and reflection properties, and provided the key required parameters in fabricating devices with similar properties.
3. POLMOD-MASCOT polarized scattering measurements can be used to predict and optimize the performance of a host of Naval operations that rely on laser imaging systems, laser communications, cameras, and other active and passive remote sensing systems
4. Determining if particulate backscattering ratios are normally spectrally independent in oceanic waters will greatly assist radiative transfer modeling efforts and the use of conversion factors to estimate backscattering from single angle backscattering devices in common use in the optics (and Naval) science community.
5. Identification of the specific Mueller matrix properties of open ocean fish that have adopted polaro-crypsis strategies can provide design principles for materials used in military operations in that environment.

RELATED PROJECTS

An NSF Award (OCE-1130793) to PI Cummings and Co-PIs Kattawar and Viktor Gruev (Washington University in St. Louis) has been funded to develop a high-resolution real-time polarization image sensor with an integrated instrument package for mooring and long-term marine deployment.

REFERENCES

Darecki M, Stramski D, Sokolski M. 2011. Measurements of high-frequency light fluctuations induced by sea surface waves with an Underwater Porcupine Radiometer System. ***J. Geophysical Res. 116***:C00H09 (http://www.agu.org/journals/jc/jc1111/2011JC007338/)

PUBLICATIONS

Sullivan, J. M., M. S. Twardowski, J. R. V. Zaneveld & C. Moore (2012) – Measuring optical backscattering in water. *Light Scattering Reviews 7: Radiative Transfer and Optical Properties of Atmosphere and Underlying Surface*, A.A. Kokhanovsky [Ed.], S Praxis Books, DOI 10.1007/978-3-642-21907-8_6, pp. 189-224. [published, refereed]

Twardowski, M., X. Zhang, S. Vagle, J. Sullivan, S. Freeman, H. Czerski, Y. You, L. Bi, G. Kattawar. (2012). The optical volume scattering function in a surf zone inverted to derive sediment and bubble particle subpopulations. Journal of Geophysical Research, 117, C00H17, doi:10.1029/2011JC007347. [published, refereed]

Gleason, A.C.R., K. J. Voss, H. R. Gordon, M. Twardowski, J. M. Sullivan, C. Trees, A. Weidemann, J. F. Berthon, D. Clarke & Z. Lee (2012) - Detailed validation of the bidirectional effect in various Case I and Case II waters. Optics Express, 20(7): 7631-7645. [published, refereed]

Gilly WF, Zeidberg LD, Booth JAT, Stewart J, Marshall G, Abernathy K, Bell L. 2012. Locomotion and behavior of Humboldt squid, *Dosidicus gigas* (d'Orbigny, 1835), in relation to natural hypoxia in the Gulf of California, Mexico *J. Exp. Biol. 215*: 3175-3190. [published, refereed]

Aurin, D. and H. M. Dierssen**.** 2012. Advantages and limitations of ocean color remote sensing in CDOM-dominated, mineral-rich coastal and estuarine waters. Remote Sensing of the Environ. 125: 181-197. [published, refereed]

Johnsen G, Z. Volent, H.M. Dierssen, R. Pettersen, M.V. Ardelan, F. Søreide, P. Fearns, M. Ludvigsen, and M. Moline. *In press*. Underwater hyperspectral imagery to create biogeochemical maps of seafloor properties. In *Subsea Optics and Imaging*. Ed. J. Watson and O. Zielinski. [published, refereed]

Hlaing S. Gilerson A, Harmel T, Tonizzo A, Weidemann A, Arnone R, Ahmed S. (2012) Assessment of a Bidirectional Reflectance Distribution Correction of Above-water and Satellite Water-leaving Radiance in Coastal Waters, *Applied Optics*, 51, 51, 220-237. [published, refereed]

Ibrahim A, Gilerson A, Harmel T, Tonizzo A, Ahmed S. (accepted) The relationship between upwelling underwater polarization and attenuation/absorption ratio, *Optics Express* [published, refereed]

Gilerson A, Ibrahim A, Harmel A, Tonizzo A, Ahmed S, (2012) Polarization techniques for the retrieval of water parameters from above and below water polarimetric observations,Proc. of SPIE 8372: Ocean Sensing and Monitoring IV, Weilin W. Hou; Robert Arnone, Editors, [published].

Tonizzo A, Gilerson A, Carrizo C, Israel J.-P., Ahmed S, (2012) Polarimetric imaging and radiometry in shallow waters, Proc. of SPIE 8364, Polarization: Measurement, Analysis, and Remote Sensing X, [published].

Harmel T, Tonizzo A, Gilerson A, Chowdhary J, Hlaing S, Ahmed S. (2011) Measuring underwater polarization field from above-water hyperspectral instrumentation for water composition retrieval, Proc of SPIE 8175: Remote Sensing of the Ocean, Sea Ice, Coastal Waters, and Large Water Regions [published].

Dierssen, H.M. and A.E. Theberge**.** In press. Bathymetry: History of Seafloor Mapping. Encyclopedia of Natural Resources. Taylor & Francis Group. New York. [in press]

Dierssen, H.M. and A.E. Theberge**.** In press. Bathymetry: Assessing Methods. Encyclopedia of Natural Resources. Taylor & Francis Group. New York. [in press]

Dierssen, H.M. and A.E. Theberge**.** In press. Bathymetry: Features and Hypsography. Encyclopedia of Natural Resources. Taylor & Francis Group. New York. [in press]

Dierssen, H.M., and Randolph, K**.** In press**.** Remote Sensing of Ocean Color. Encyclopedia of Sustainability Science and Technology. Springer-Verlag. [in press]

Brady P, Travis K, Maginnis T, Cummings ME. *submitted*, The polaro-cryptic mirror: an example of biological engineering for open-ocean camouflage. *Nature Photonics*

Meng Gao, Yu You, Ping Yang, and George W. Kattawar, *submitted*, Backscattering Properties of Small Layered Plates: A Model for Iridosomes. *Optics Express.*

HONORS/AWARDS/PRIZES

George Kattawar will be honored in a special issue of Applied Optics Honoring the 50 most prolific authors in the past 50 years as the #4 most prolific. A link to this issue can be found at http://www.opticsinfobase.org/ao/journal/ao/anniversary/50mostpublished.cfm).

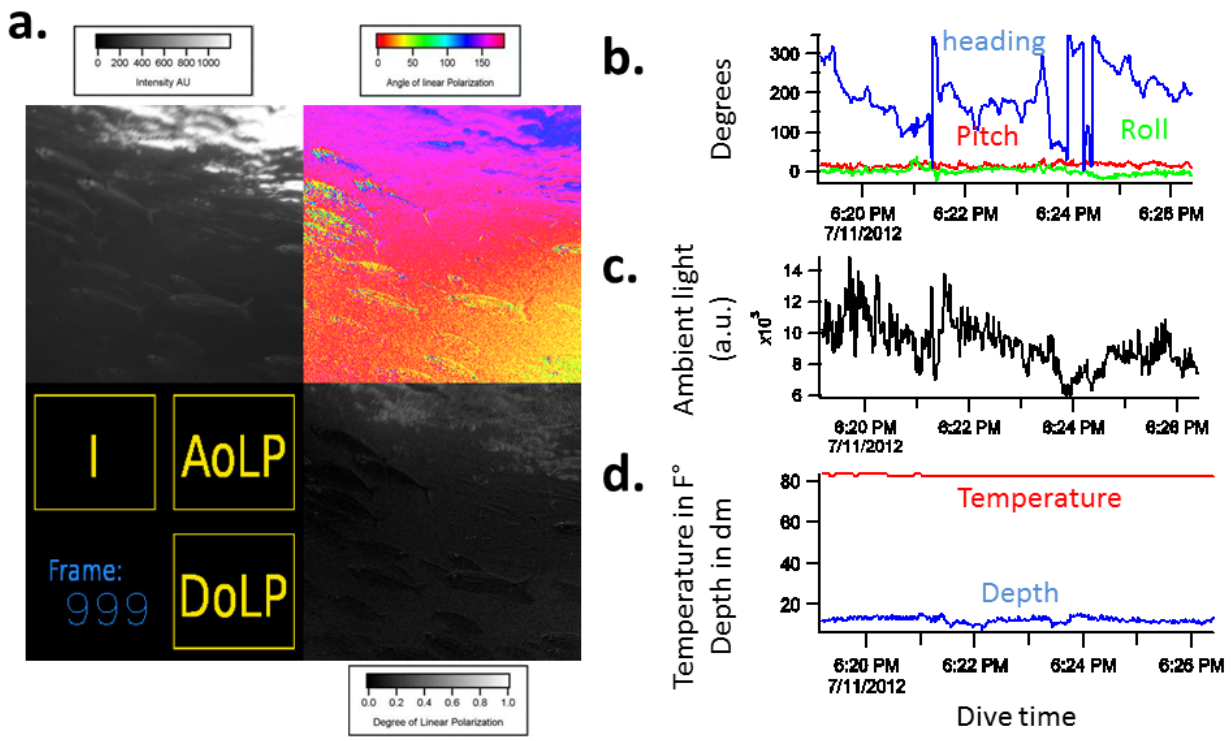

Figure 1. Video polarimetery data of a school of BigEyed Scad in Curacao showing intensity (I), angle of polarization (AoLP), and degree of polarization (DoLP) (a.) with associated sensor package data featuring compass heading, camera pitch, camera roll (b.), ambient light (c.), temperature, and depth (d.).

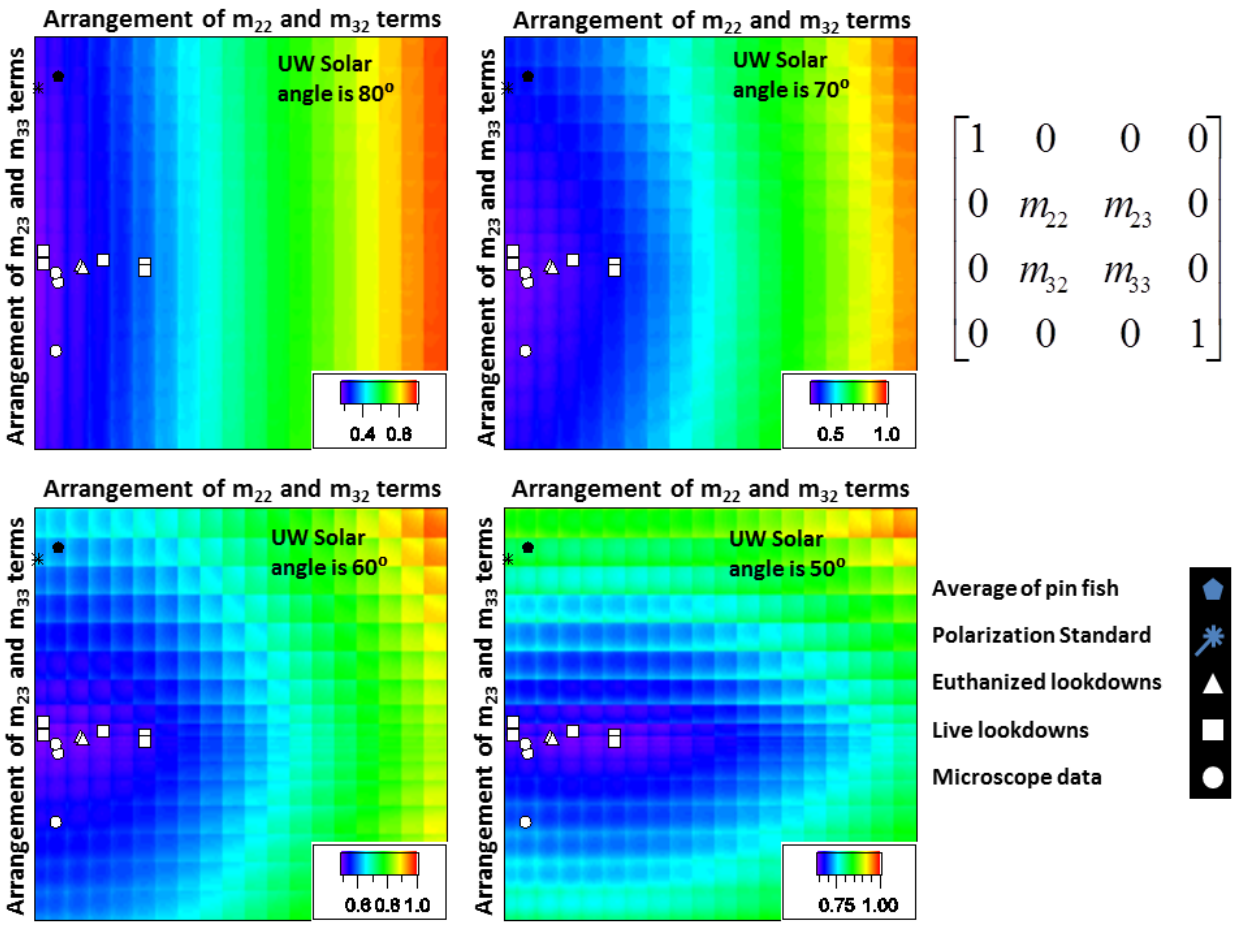

Figure 2. Polaro-Crypsis in the open ocean. The color map represents the polarization contrast graphed over a specialized map of the inner four terms of the Muller matrix where cooler colors (blue) represent maximal polaro-crypsis. The polarization contrast is summed over the full 360° horizontal predator angles with the fish heading angle summed over -80° to 80° with respect to the predator location. The maximum DoLP was .6. Triangle, circle, and square points are projected points of the euthanized, microscope measured, and live Lookdowns (an open ocean fish species) respectively, with each point representing an individual fish. The star point is the polarization standard (~ representing a vertical mirror strategy), and the pentagon point is the average of live pinfish (a seagrass dwelling fish) measurements in the same set up as the live Lookdowns.

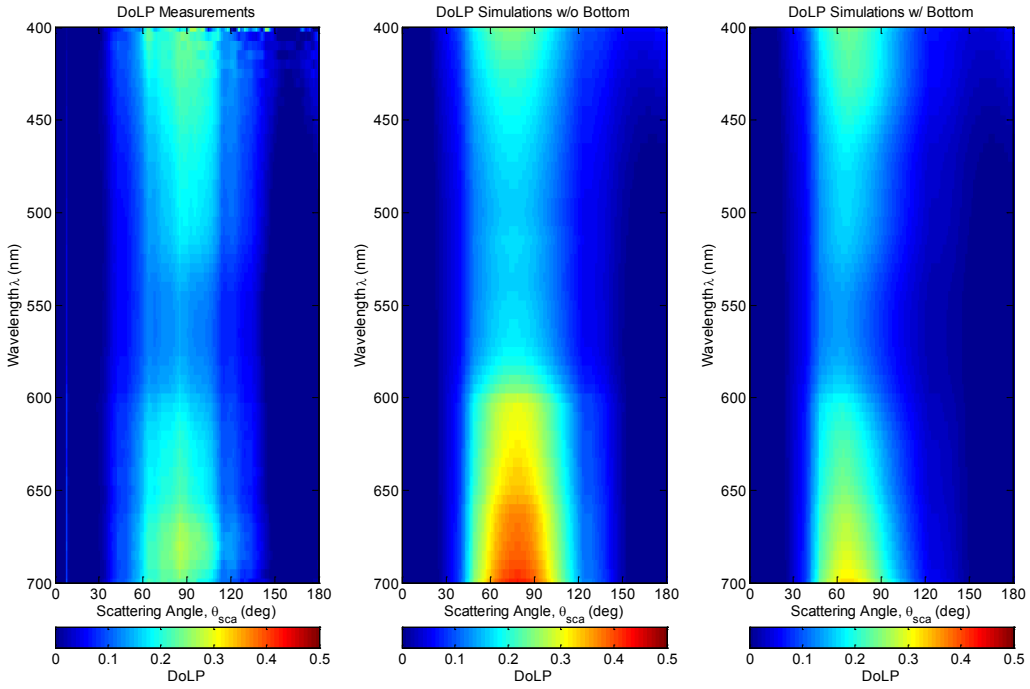

Figure 3. Detailed comparison of the hyperspectral polarization characteristics of light in shallow waters (Florida Keys, January and August 2011) measured by the CCNY polarimeter and simulated by radiative transfer (RT) code RayXP based on measured IOPs (WET Labs) was made for 4 water sites, various sun conditions, azimuth orientations and depths. Hyperspectral distribution of the degree of polarization measured by the polarimeter (left), simulated assuming no bottom (center) and assuming Lambertian, non-polarized bottom (Tonizzo et al., in preparation).

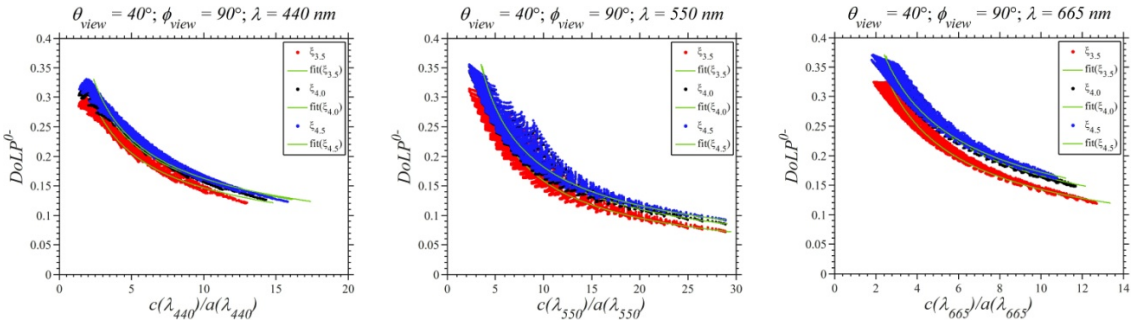

Figure 4. Relationship between DoLP and attenuation/absorption ratio at 440, 550 and 665 nm, at θview = 40° for three different NAP slopes of the particle size distribution (PSD). (Ibrahim, et al. (accepted) Optics Express.

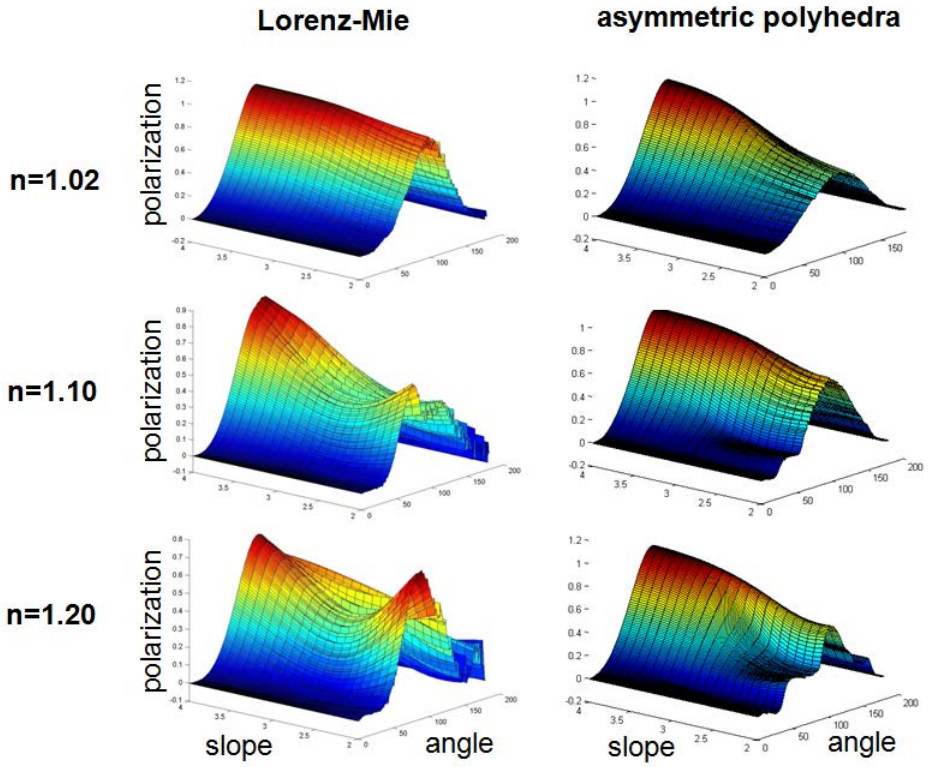

Figure 5. The modeled degree of linear polarization (polarization) as a function of particle size distribution slope (slope) and VSF angle (angle) for spherical (Lorenz-Mie) and non-spherical (asymmetric polyhedra) particle populations with three different refractive indices (n).

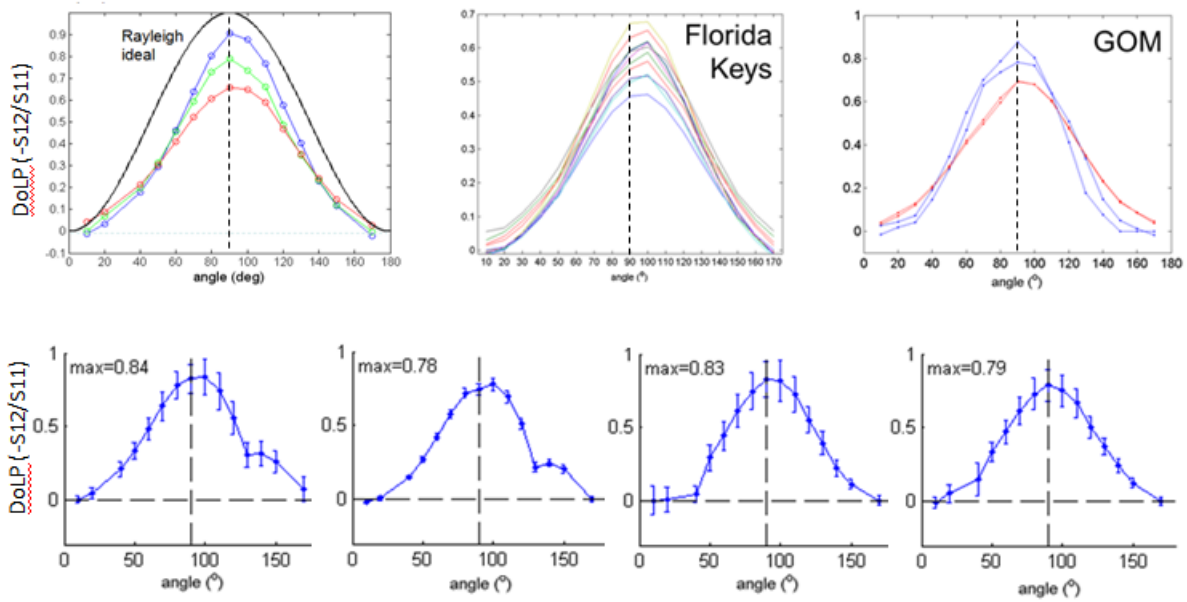

Figure 6. Example of the variability in the degree of linear polarization (DoLP) for natural particle populations collected at various field sites.

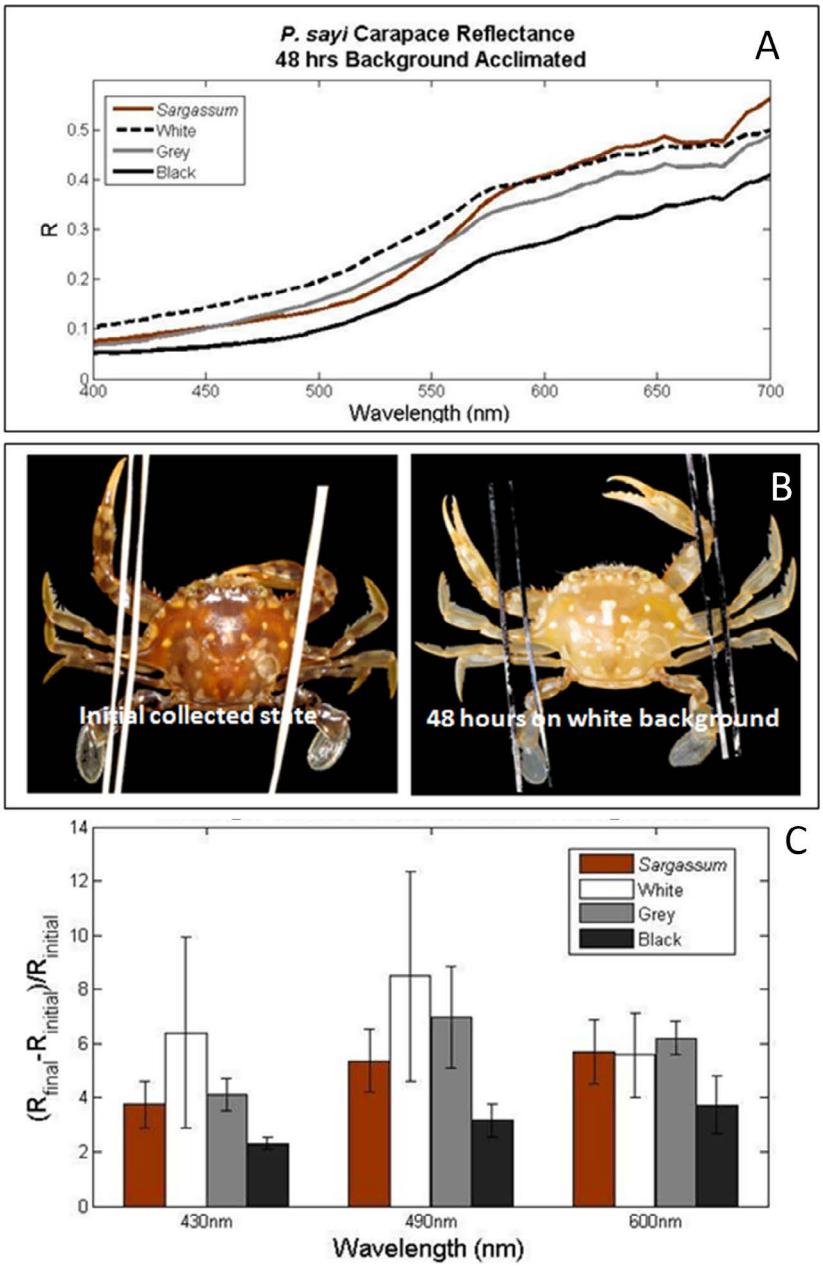

Figure 7. A) Mean carapace reflectance for P. sayi kept on artificial colored substrates for 48 hours. Crabs on black had the lowest overall reflectance, with grey and control (live Sargassum) groups approximately equal over most of the visible. –B) Individual P. sayi after being removed from holding on Sargassum (left) and after 48 hours on white background (right) C) Change in mean reflectance $(R_{Final}/R_{Initial})/R_{Initial}$ after 48 hours for all treatments. Three biologically relevant wavelengths are considered: 430nm (within visual range of most predators), 490nm (likely crab visual maxima) and 600nm (high reflectance for crabs and algae). Error bars represent +/- 1 standard deviation.

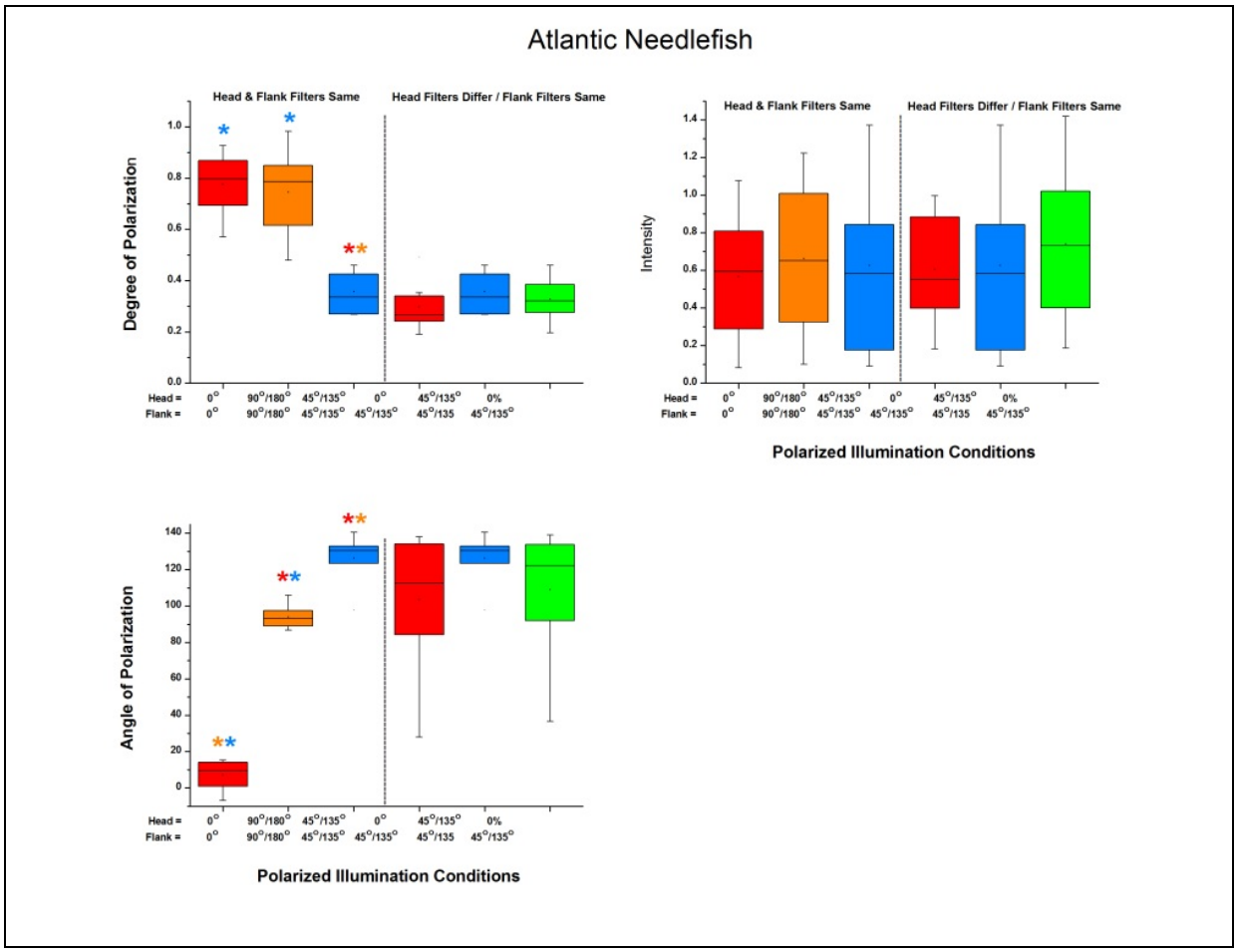

Figure 8. Atlantic needlefish Polarization reflectance measurements. The left side of each panel represents measurements when the fish's visual system is presented with the same angle of incident polarization as the flank. The right side indicates changing visual conditions when the flank conditions remain the same.

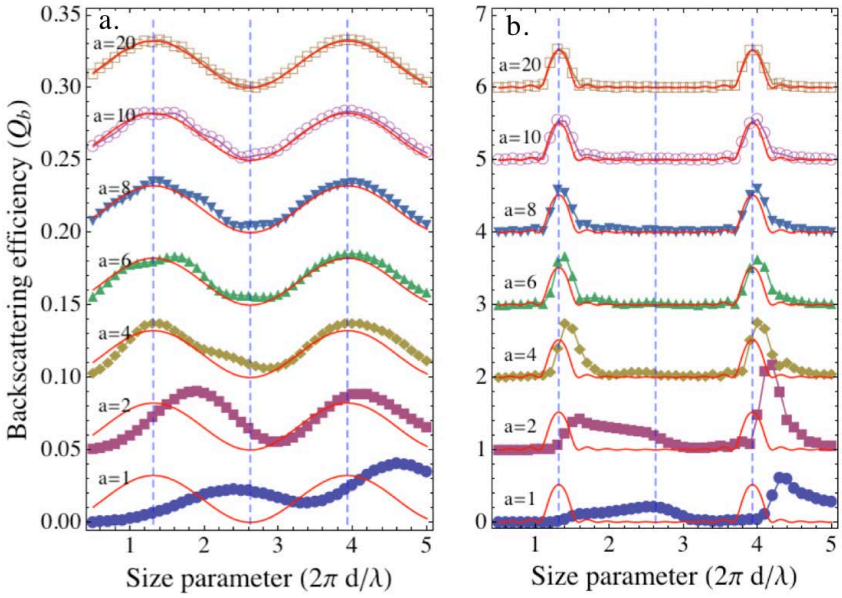

Fig.9. Backscattering efficiency Qb versus size parameter $x = 2\pi d / \lambda$ ***of the plate thickness at different aspect ratios under normal incidence. The reflection for semi-infinite plates is indicated by solid red lines. (a) Results for a single-layer plate. Each curve is successively moved upward by 0.05. Maximum reflection of the semi-infinite plates is 0.033 at x=1.3 and 3.9. (b) Results for 5-layer plate. Each curve is successively moved upward by 1.0. To use the reflection of semi-infinite plates to approximate the backscattering efficiency (within 10% error), for single-layer plates, the aspect ratio must be larger than 4, and for 5-layer plates, the aspect ratio must be larger than 8.***

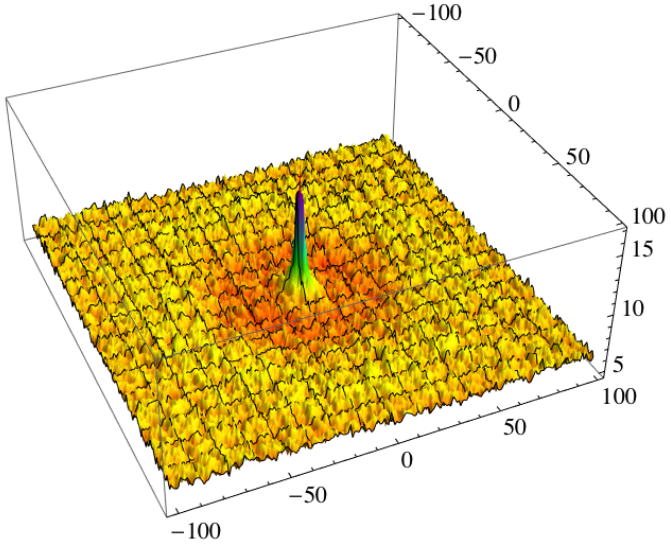

Fig. 10 . Fourier spatial power spectrum of leucosomes, obtained by using DFT analysis on the leucosome position data (measured by Stephen Senft and Alan M. Kuzirian, MBL). The only prominent peak at the zero frequency point suggested that there is no spatial correlation between leucosomes.

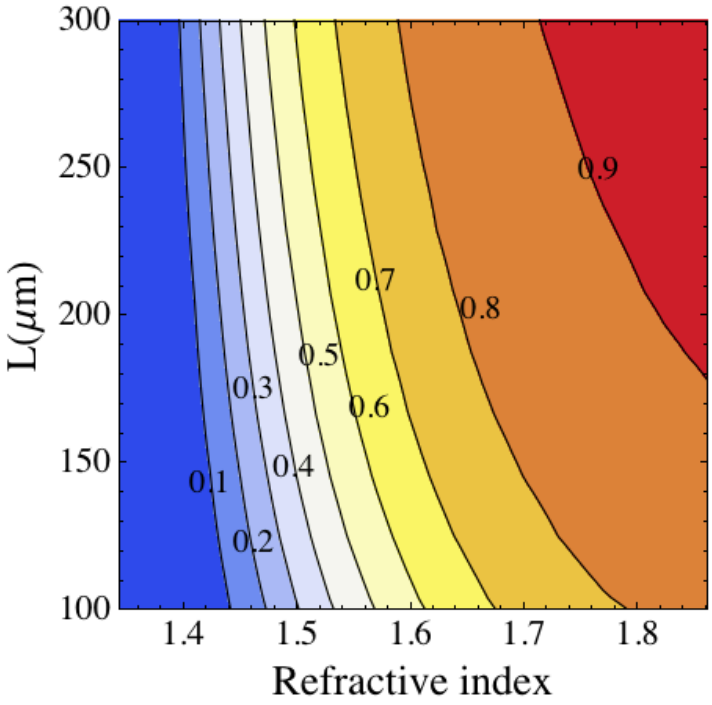

Fig 11. Contour plot of the reflectance versus refractive index (x-axis) and thickness (y-axis). Modeling results suggest theoretical refractive index between 1.50 and 1.54 for a leucophore system of a thickness between 100μm to 300μm (measured by Stephen Senft and Alan M. Kuzirian, MBL) and reflectance between 30% to 70% (measured by Lydia Mathger, MBL).

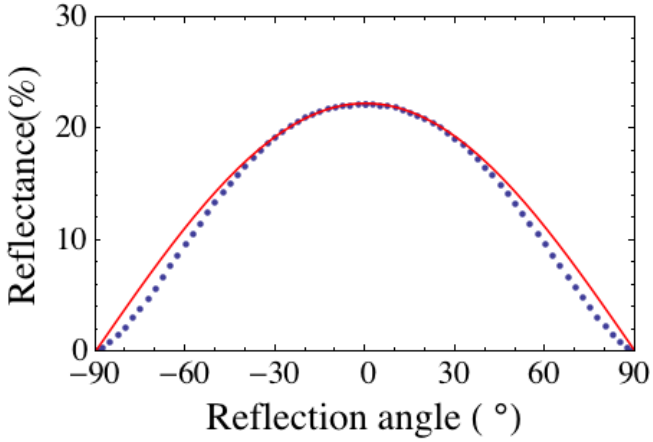

Fig 12. Modeled angular reflectance for refractive index n=1.513 and thickness L=300μm at 0° incident angles. The angular distribution is almost a cosine function, (denoted by the red solid line) typical of a Lambertian surface.

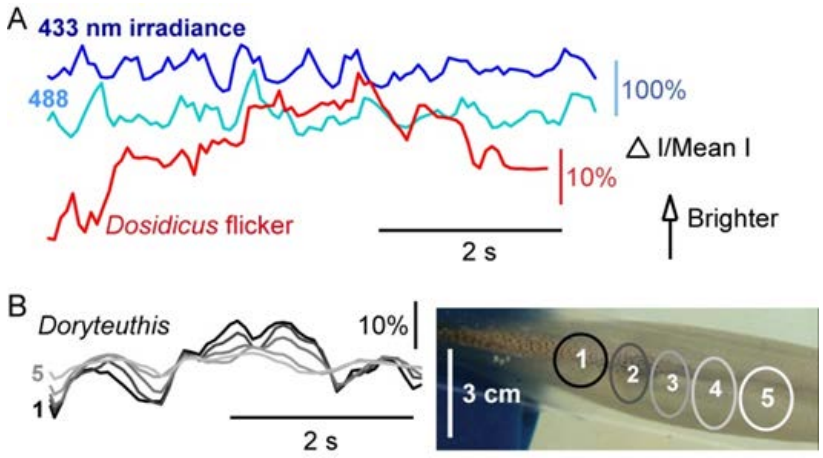

Figure 13. Temporal characteristics of flickering in living Dosidicus and Doryteuthis. (A) Flickering in Dosidicus at 35 m depth (Sept. 2009) compared to the fluctuations (ΔI) in intensity (I) of downwelled blue light (433 nm and 488 nm) at 7 m depth in the Gulf of California (June, 2011; M. Darkecki and D. Stramski, unpublished data; see Darecki et al., 2011). Flickering was measured from Cirttercam video recordings of the dorsal surface of the camera-bearing squid's head (Gilly et al. 2012) as average gray-scale values of a patch of skin (15 Hz frame rate). Light was sampled at 1 KHz and subsampled by averaging 20 points every 0.0667 s to match the shutter speed (1/50 s) and frame rate of the Crittercam. Values were normalized by the mean of the time series (ΔI/Mean I). The two traces were manually aligned in an arbitrary way to visualize temporal similarities. (B) Flickering-like chromatophore activity in Doryteuthis was recorded in a cylindrical chamber with a Sony camcorder (May, 2012). The five traces correspond to the regions indicated on the right (1 is most posterior). Grayscale values were measured using ImageJ and normalized by the mean to match the vertical units (ΔI/Mean I) used in panel A. Loosely coupled and irregular fluctuations are apparent. We propose that background flickering may also occur in Doryteuthis, but its exact temporal-spatial characteristics, biological function and relative importance of vertical vs. horizontal control are not identical to the corresponding properties in Dosidicus.

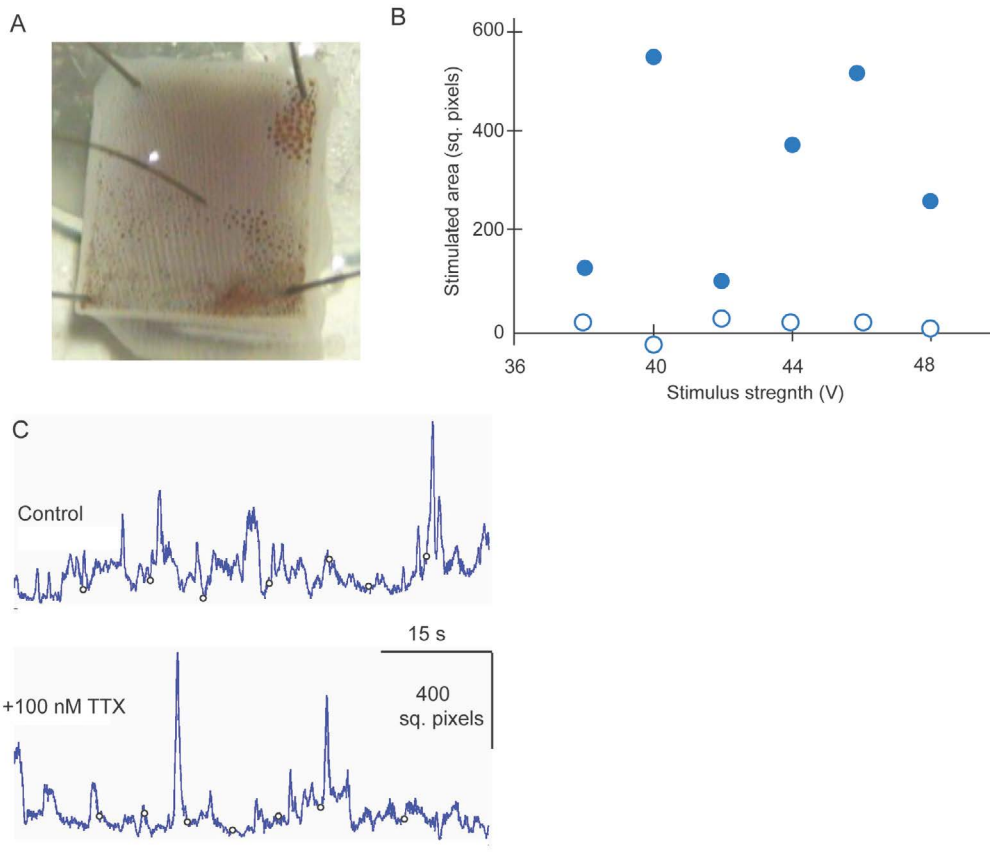

Figure 14 (A) Preparation of a piece of excised Sthenoteuthis fin (2 x 2 cm) positioned ventral-side up for stimulation experiments. The tip of the coaxial, bipolar electrode is in the center of the frame. Experiments were carried out at room temperature of 20-22 °C on board the RV Kilo Moana off the coast of Hawaii. (B) Effect of TTX on stimulated chromatophore activity. The area of active chromatophores was graded with stimulus strength when the fins were bathed in seawater (filled circles). Addition of TTX (100nM) blocked stimulated activity (open circles). Results are typical of 10 experiments. (C) Effects of TTX on spontaneous, propagated chromatophore activity. Open circles indicate stimuli. Spontaneous activity of this sort persisted in the presence of 100 nM TTX with no noticeable change in amplitude, frequency of individual events, area of activated chromatophores or the nature of propagation.

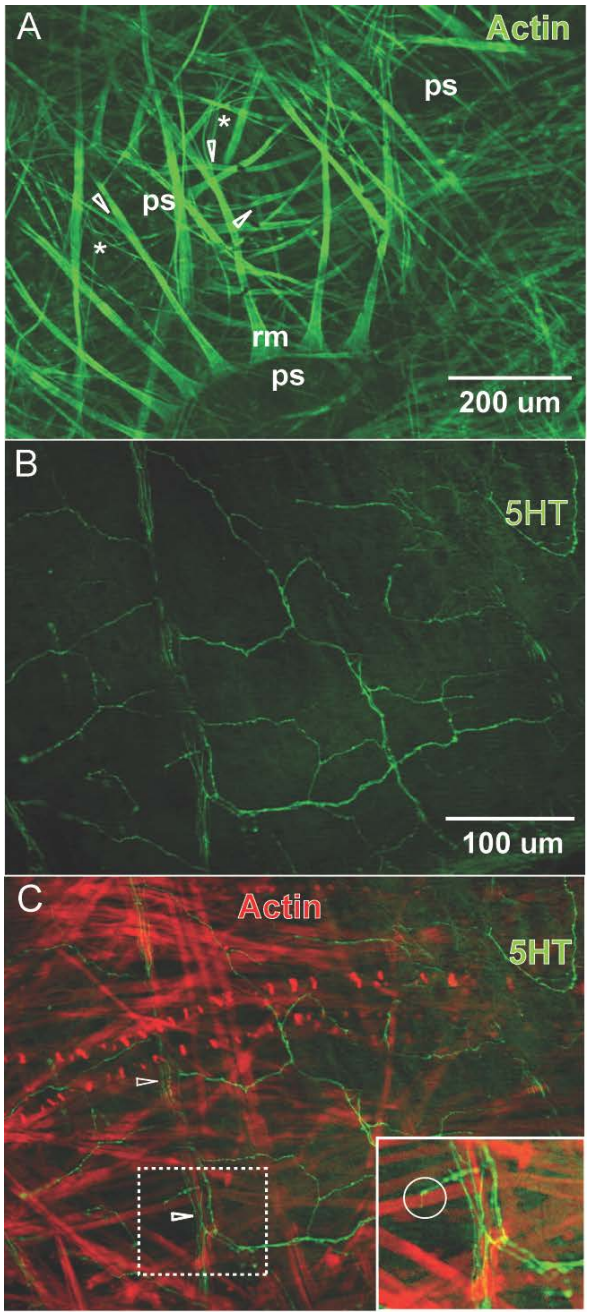

Figure 15. Fluorescently labeled muscular and neural elements in skin of Doryteuthis. Skin was fixed in 4% paraformaldehyde in Ca-free artificial sea water (ASW): (in mM) 480 NaCl, 10 KCl, 20 $MgCl_2$, 20 $MgS0_4$, 10 Hepes (pH 7.8) for 4 hours at room temperature, washed overnight in Ca-free ASW and then in standard PBS. Whole-mounts of flat pieces of intact skin were cleared in glycerol and imaged using a Zeiss AxioImager Z1 microscope(10x (panel A) and 20x objective (Panel B) with Aptome and Axiovision software that allows analysis of optical sections (2-3 um thick in A; 1-2 um thick in B,C).This work was done with C. Lowe at Hopkins Maine Station.

(A) Actin labeling with Alexa Fluor 488 phalloidin. Three chromatophore pigment sacs (ps) in slightly different vertical planes are visible with attached radial muscle fibers (rm). Arrowheads indicate branch-points of muscle fibers; branching appears to be common. Asterisks indicate putative multipolar cells that may serve to provide attachment points for several radial muscle fibers.

(B) Serotonin (5HT) immuno-labeling with anti-5HT primary antibodies (rabbit, Sigma) and Alexa Fluor 546 anti-rabbit secondary antibody. A prominent network of presumptive neural processes containing 5HT is evident. Neuronal cell bodies, as would be expected in a peripheral nerve net, are not obvious. Scale bar applies to panels B and C.

(C) Superimposed images of actin and 5HT labeling as described above for the same region as shown in panel B. Identity of actin-labeled presumptive muscle fibers are not clear, but presumably most are processes of radial muscle fibers. 5HT-containing presumptive axons approach muscle fibers and from a basket-like enclosure (arrowheads). An apparent axonal termination on a muscle fiber is shown in the circle in the inset. One axon sends a small process around a muscle fiber, ensnaring it in a ring-like arrangement. This contact region was limited to a few optical sections. Other images (not illustrated) show 5HT-containing processes that approach the base of a radial muscle fiber at a pigment sac and course along the muscle fiber for a short distance before meandering off. Whether these axons also contain the excitatory neuromuscular transmitter (glutamate) or other modulatory compounds (e.g. FMRFamide or Ach) is unknown.

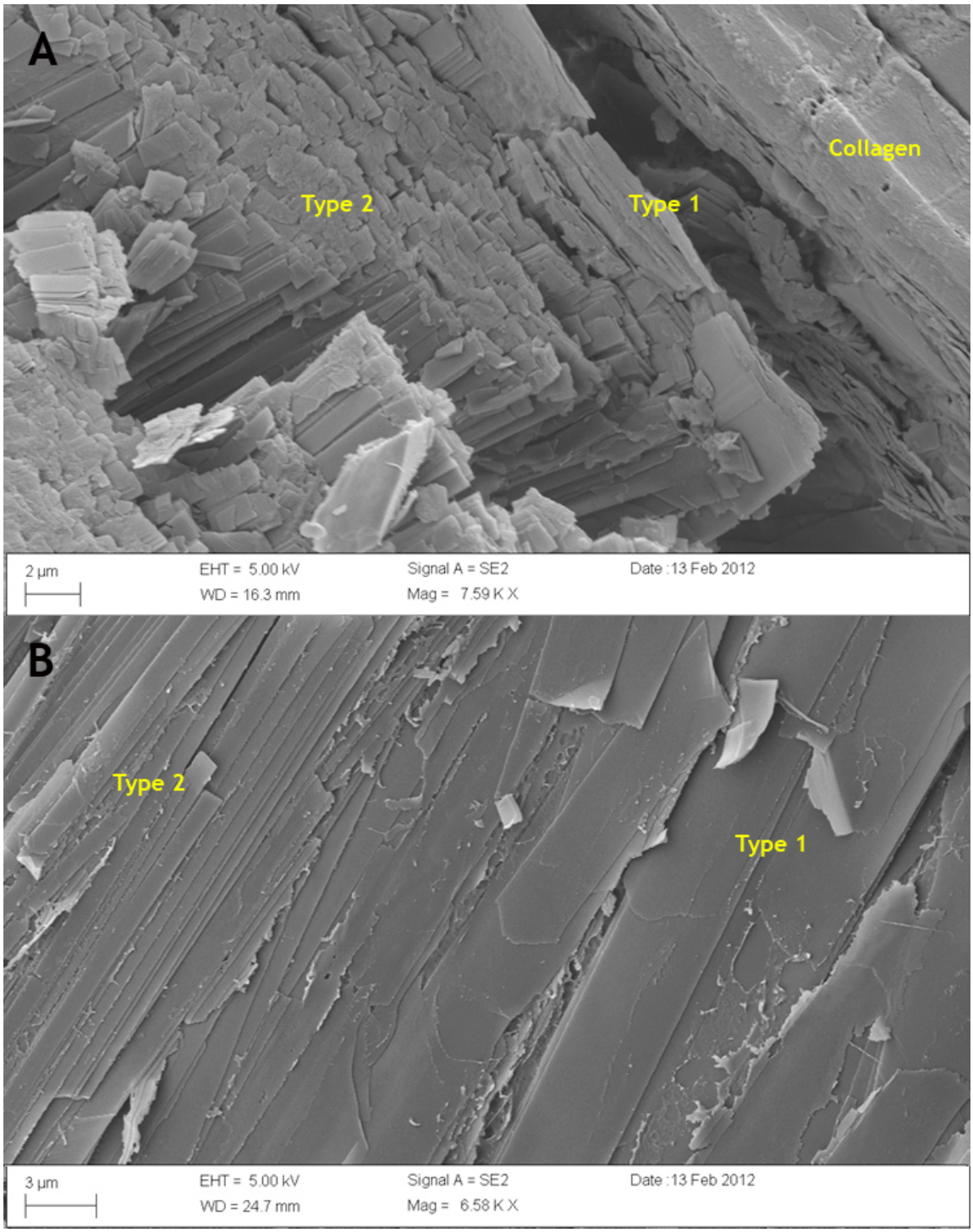

Figure 16: SEM of the iridophore layer from the mid-flank region of the lookdown. A horizontal section (A) shows two different types of iridophores (Type 1 and Type 2) in the dermis. A horizontal plane is parallel to the anterior-posterior axis and divides the fish into the dorsal and ventral parts. A parasagittal section (B) shows Type 1 and Type 2 iridophores with wider (~3-5 µm) and thinner (~1 µm or less) guanine platelets, respectively. A sagittal plane is a vertical plane that contains the anterior-posterior axis and divides the fish into left and right halves. A parasagittal plane is parallel to the sagittal plane but does not go through the anterior-posterior axis.

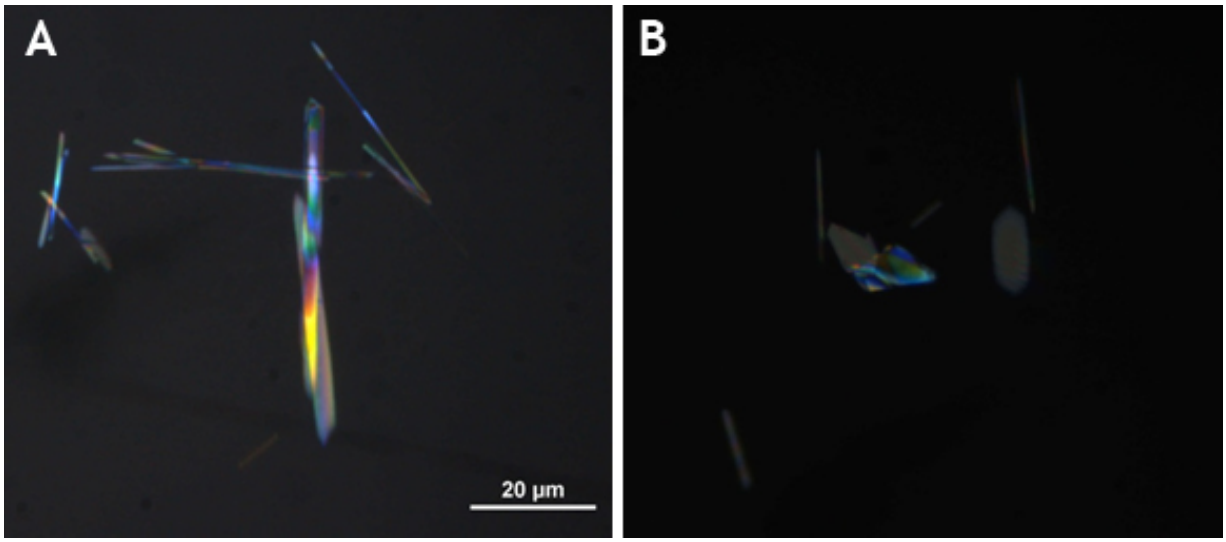

Figure 17. Light microscopic images of dissociated guanine platelets from the mid-flank (A) and the dorsal (B) regions of the lookdown skin. The Type 2 iridophores in the dorsal region have much wider but shorter guanine platelets than those in the mid-flank region. The average dimensions of the large (Type 1) and the samll (Type 2) guanine platelets in the mid-flank region are approximately 5 x 30 µm and 1 x 30 (µm), respectively. The average dimensions of the large (Type 1) and the samll (Type 2) guanine platelets in the dorsal region are approximately 8 x 16 µm and 1 x 14 µm, respectively.